No. 663 **May 2023**

FEM Modeling And Simulation of Thixo-viscoplastic Flow Problems

N. Begum, A. Ouazzi, S. Turek

ISSN: 2190-1767

FEM Modeling And Simulation of Thixo-viscoplastic Flow Problems

Naheed Begum*, Abderrahim Ouazzi, and Stefan Turek

Institute for Applied Mathematics and Numerics, LSIII, TU Dortmund University, Vogelpothsweg 87, D-44227 Dortmund, Germany.

** Corresponding author:naheed.begum@tu-dortmund.de*
Abderrahim.Ouazzi@math.tu-dortmund.de
Stefan.Turek@math.tu-dortmund.de

Abstract. We are concerned, in this work, with Finite Element Method (FEM) for modeling and simulation of thixotropy in viscoplastic materials. We use a quasi-Newtonian approach to integrate the constitutive equation, which results in a new thixo-viscoplastic (TVP) generalized Navier-Stokes (N-S) equations. To solve the corresponding flow fields at once, we developed a FEM TVP solver based on monolithic Newton-multigrid method. The phenomenological process of competition of breakdown and buildup characteristics of thixotropic material is replicated throughout, localization and shear banding for Couette flow on one hand, and induction of more shear rejuvenation layers nearby walls for contraction flow on the other hand.

Keywords: Thixo-viscoplastic, Localization, Shear banding, TVP generalized Navier-Stokes equations, FEM, Newton-multigrid, Local pressure Schur complement, Couette flow, 4:1 contraction

INTRODUCTION

We intend to investigate thixotropy in fluid flow problems with the lens of modeling, simulation, and optimization, as pillars for studying rheological phenomena using computer experiments.

We use FEM quasi-Newtonian modeling approach to incorporate the internal material microstructure via structure dependent viscosity. This is a natural way to generalize Finite element settings of N-S equations to include complex rheological phenomena. As, the constitutive equation cohabits shear-rate independent and shear-rate dependent stress behaviours, we analyze the type of transitions between fluid-like and solid-like regimes for Couette flow to manifest the competition process of breakdown and buildup for thixotropic material. Furthermore, we consider 4:1 contraction flow to investigate the impact of thixotropy on flow distribution in the vicinity of walls for an eventual optimal settings of restart pressure.

The quasi-Newtonian modeling approach requires a robust solver w.r.t. regularization parameter to obtain accurate numerical solutions. In this regard, we develop a corresponding adaptive combined discrete Newton's/monolithic geometric multigrid solver to delicately handle the regularization issue. On one hand, the adaptivity related to discrete Newton's is due to the adaptive step-size in divided difference for the Jacobian calculation, while accuracy/convergence of linear multigrid solver is made dependently on accuracy/convergence of nonlinear solver. On other hand, we use Local Pressure Schur Complement (LPSC) to handle linearized saddle point problems inside the outer Newton sweeps, taking in consideration the advantageous aspect of discontinuous linear pressure FEM approximation. We collocate velocity and structure parameter with the same FEM quadratic interpolation.

The remainder of the paper is structured as follows, we devote section §2 to quasi-Newtonian modeling approach for TVP flow problems via regularized viscosity and give the corresponding set of TVP equations. Then, in section §3, we provide the wellposedness results for TVP problem and establish the best approximation, followed by the finite element approximations and the necessary stabilization. We solve the resulting discrete system with an adaptive combined discrete Newton's/monolithic geometric multigrid solver in section §4. Then, we investigate thixotropy rheological phenomena for two flow configurations in section §5, namely, Couette flow as a simple enough for modeling and 4:1 contraction flow as a close enough to industrial application. In section §6, we highlight conclusions and main results of the paper.

QUASI-NEWTONIAN MODELING APPROACH

In this section, we introduce quasi-Newtonian modeling approach for TVP flows. This is a straightforward way to use Navier-Stokes equations, as a long standing tool for modeling and simulations of incompressible

flow problems [1, 2]. The extended viscosity, $\mu(\cdot,\cdot)$, dependent on shear rate, $\|\mathbf{D}\|$, and microstructure, λ, for the generalized TVP Navier-Stokes equations uses an approximation for $\|\mathbf{D}\|^{-1}$. Papanastasiuo regularization [3], for instance:

$$\frac{1}{\sqrt{D_{\mathrm{II},r}}} := \frac{1}{\sqrt{D_{\mathrm{II}}}}\left(1 - e^{-k\sqrt{D_{\mathrm{II}}}}\right), \tag{1}$$

where k is a regularization parameter, and $D_{\mathrm{II}} = \frac{1}{2}\left(\mathbf{D}(\boldsymbol{u}) : \mathbf{D}(\boldsymbol{u})\right)$ is second invariant of rate-of-strain tensor $\mathbf{D}(\boldsymbol{u})$. Then, the full set of equations for TVP generalized Navier-Stokes problems reads

$$\begin{cases} \left(\dfrac{\partial}{\partial t} + u\cdot\nabla\right)\boldsymbol{u} - \boldsymbol{\nabla}\cdot\left(2\mu(D_{\mathrm{II},r},\lambda)\mathbf{D}(\boldsymbol{u})\right) + \nabla p = \boldsymbol{f}_{\boldsymbol{u}}, \\ \nabla\cdot\boldsymbol{u} = 0, \\ \left(\dfrac{\partial}{\partial t} + u\cdot\nabla\right)\lambda + \mathcal{M}(D_{\mathrm{II}},\lambda) = f_\lambda, \end{cases} \tag{2}$$

in Ω. We denote flow fields, microstructure, velocity, and pressure, by λ, $\boldsymbol{u}$, and p, respectively, and body forces by f_λ and $\boldsymbol{f}_{\boldsymbol{u}}$. The viscosity in (2) is defined as

$$\mu(D_{\mathrm{II},r},\lambda) = \eta(D_{\mathrm{II}},\lambda) + \tau(\lambda)\frac{\sqrt{2}}{2}\frac{1}{\sqrt{D_{\mathrm{II},r}}} \tag{3}$$

The additional equation for λ in (2) is responsible to integrate breakdown, $\mathcal{G}$, and buildup, $\mathcal{F}$, competition process. We concisely define TVP model as

$$\mathcal{M} := \mathcal{G} - \mathcal{F}. \tag{4}$$

We summarize from literature a bunch of models in Table I.

TABLE I. Models for thixotropic materials

	η	τ	$\mathcal{F}$	$\mathcal{G}$
Worrall et al. [4]	$\lambda\,\eta_0$	τ_0	$\mathcal{M}_a(1-\lambda)\,\|\mathbf{D}\|$	$\mathcal{M}_b\lambda\,\|\mathbf{D}\|$
Coussot et al. [5]	$\lambda^g\,\eta_0$		$\mathcal{M}_a$	$\mathcal{M}_b\lambda\,\|\mathbf{D}\|$
Houška [6]	$(\eta_0+\eta_\infty\lambda)\,\|\mathbf{D}\|^{n-1}$	$(\tau_0+\tau_\infty\lambda)$	$\mathcal{M}_a(1-\lambda)$	$\mathcal{M}_b\lambda^m\,\|\mathbf{D}\|$
Dullaert et al. [7]	$\lambda\eta_0$	$\lambda G_0(\lambda\,\|\mathbf{D}\|)\Lambda_c$	$(\mathcal{M}_{a_1}+\mathcal{M}_{a_2}\,\|\mathbf{D}\|)(1-\lambda)t^p$	$\mathcal{M}_b\lambda\,\|\mathbf{D}\|\,t^{-p}$

Buildup parameter, $\mathcal{M}_a$, breakage parameter, $\mathcal{M}_b$, nonthixotropic plastic viscosity, η_0, nonthixotropic yield stress, τ_0, thixotropic plastic viscosity, η_∞, thixotropic yield stress, τ_∞, critical elastic strain, Λ_c, elastic modulus of unyielded material G_0, and indices rate g, p, m, n give rise to different thixotropic models.

FINITE ELEMENT APPROXIMATIONS

We devote this section to FEM approximation of TVP problem by a simple generalization of classical FEM settings of N-S equations. Firstly, we give the weak form of the problem in its general saddle point abstract framework based on incompressibility. Secondly, we demonstrate the wellposedness of TVP problem and give the boundedness of solutions w.r.t. data. Thirdly, we present the best approximation, where the energy estimate shows nonoptimality due to weak coercivity of microstructure. Lastly, we introduce FEM spaces choice respecting the incompressibility constraint only, while microstructure is collocated with the same FEM approximation as velocity with the necessary stabilization to cope mainly with weak coercivity.

We consider the spaces $\mathbb{V} := (H_0^1(\Omega))^2$ and $\mathbb{Q} := L_0^2(\Omega)$ for velocity and pressure, respectively. And the space $\mathbb{T} := H^1_{\Gamma^-}(\Omega)$ for microstructure, where Γ^- denotes the inflow boundary. We associate spaces $\mathbb{T}$ and $\mathbb{V}$ with H^1-norm $\|\cdot\|_1$ and $\mathbb{Q}$ space with L^2-norm $\|\cdot\|_0$, and set $\mathbb{W} := \mathbb{V}\times\mathbb{T}$ [8]. We define on $\mathbb{W}\times\mathbb{W}$

$$a_{\tilde{\boldsymbol{u}}}(\tilde{\boldsymbol{u}})(\tilde{\boldsymbol{u}},\tilde{\boldsymbol{v}}) = a_{\boldsymbol{u}}(\tilde{\boldsymbol{u}})(\boldsymbol{u},\boldsymbol{v}) + a_\lambda(\tilde{\boldsymbol{u}})(\lambda,\xi) \quad \text{for all } (\tilde{\boldsymbol{u}},\tilde{\boldsymbol{v}})\in\mathbb{W}\times\mathbb{W}, \tag{5}$$

where, $\tilde{\boldsymbol{u}} = (\lambda,\boldsymbol{u})$ and $\tilde{\boldsymbol{v}} = (\xi,\boldsymbol{v})$.

The continuous weak form of TVP problem (2), in saddle point abstract framework based on incompressibility, reads: *Find* $(\tilde{\boldsymbol{u}},p)\in\mathbb{W}\times\mathbb{Q}$ *such that*

$$a_{\tilde{\boldsymbol{u}}}(\tilde{\boldsymbol{u}})(\tilde{\boldsymbol{u}},\tilde{\boldsymbol{v}}) - b(\boldsymbol{u},q) + b(\boldsymbol{v},p) = l(\tilde{\boldsymbol{v}}) \quad \text{for all } (\tilde{\boldsymbol{v}},q)\in\mathbb{W}\times\mathbb{Q}, \tag{6}$$

where

$$a_{\boldsymbol{u}}(\tilde{\boldsymbol{u}})(\boldsymbol{u},\boldsymbol{v}) = \int_\Omega \boldsymbol{u}\cdot\nabla\boldsymbol{u}\,\boldsymbol{v}\,d\Omega + \int_\Omega 2\mu(D_{\mathrm{II}},\lambda)\mathbf{D}(\boldsymbol{u}):\mathbf{D}(\boldsymbol{v})\,d\Omega, \tag{7}$$

$$b(\boldsymbol{v},q) = -\int_\Omega \nabla\cdot\boldsymbol{v}\,q\,d\Omega, \tag{8}$$

$$l_{\boldsymbol{u}}(\boldsymbol{v}) = \Big(\boldsymbol{f}_{\boldsymbol{u}},\boldsymbol{v}\Big), \tag{9}$$

$$a_\lambda(\tilde{\boldsymbol{u}})(\lambda,\xi) = \int_\Omega \boldsymbol{u}\cdot\nabla\lambda\,\xi\,d\Omega + \int_\Omega \Big(\mathcal{G}(D_{\mathrm{II}},\lambda) - \mathcal{F}(D_{\mathrm{II}},\lambda)\Big)\,\xi\,d\Omega, \tag{10}$$

$$l_\lambda(\xi) = \Big(f_\lambda,\xi\Big), \text{ and set } l(\tilde{\boldsymbol{v}}) = l_\lambda(\xi) + l_{\boldsymbol{u}}(\boldsymbol{v}). \tag{11}$$

In theorem 1, we state the results concerning wellposedness and boundedness of solutions w.r.t. data. We assume

$$\eta_0\mathcal{C}_K - \mathcal{C}_1\,|\boldsymbol{u}|_1 > 0 \tag{12}$$

$$\mathcal{M}_a - \mathcal{C}_2\mathcal{M}_b\,|\boldsymbol{u}|_{1,\infty} > 0 \tag{13}$$

where $\mathcal{C}_i$, i=1,2 are continuity constants related to, convective term in momentum equation and thixotropy build up function, respectively.

Theorem 1 (Begum et. al 2022 [8]). *Given $f_\lambda \in L^2(\Omega)$, $\boldsymbol{f}_{\boldsymbol{u}} \in (L^2(\Omega))^2$, and assume conditions (12) and (13) are satisfied. Then, TVP problem (6) has a unique solution $(\tilde{\boldsymbol{u}},p) = (\lambda,\boldsymbol{u},p) \in \mathbb{W}\times\mathbb{Q}$. Furthermore, the solution satisfies the boundedness with data*

$$\|\boldsymbol{u}\|_1 \leq \frac{1}{\eta_0\mathcal{C}_K}\,\|\boldsymbol{f}_{\boldsymbol{u}}\|_0 \tag{14}$$

$$\|p\|_0 \leq \frac{1}{\beta}\Big(1 + \frac{2\,(\eta_\infty + k\tau_\infty) + \|\boldsymbol{u}\|_\infty}{\eta_0\mathcal{C}_K}\Big)\,\|\boldsymbol{f}_{\boldsymbol{u}}\|_0 \tag{15}$$

$$\mathcal{M}_a\,\|\lambda\|_0^2 + \frac{1}{2}\langle\lambda\rangle^2 \leq \frac{1}{\mathcal{M}_a}\,\|f_\lambda\|_0^2 \tag{16}$$

where β denotes LBB constant, and $\mathcal{C}_K$ is the constant of Korn's inequality.

The upper norm bound for microstructure solution is composed of boundary norm and L^2-norm (16), i.e. the high order derivative of λ is not controlled, which is due to weak coercivity. This coarseness is reflected in the best approximation of the approximate problem.

Now, we introduce spaces for approximations in a conforming framework $\mathbb{W}_h := \mathbb{V}_h\times\mathbb{T}_h \subset \mathbb{V}\times\mathbb{T}$ and $\mathbb{Q}_h \subset \mathbb{Q}$. The corresponding discrete TVP problem is to look for a solution $(\tilde{\boldsymbol{u}}_h,p_h) \in \mathbb{W}_h\times\mathbb{Q}_h$ such that

$$a_{\tilde{\boldsymbol{u}}}(\tilde{\boldsymbol{u}}_h)(\tilde{\boldsymbol{u}}_h,\tilde{\boldsymbol{v}}_h) - b(\boldsymbol{u}_h,q_h) + b(\boldsymbol{v}_h,p_h) = l(\tilde{\boldsymbol{v}}_h) \quad \text{ for all } (\tilde{\boldsymbol{v}}_h,q_h) \in \mathbb{W}_h\times\mathbb{Q}_h. \tag{17}$$

Theorem 2 (Begum et. al 2022 [9]). *Let $\boldsymbol{f}_{\boldsymbol{u}} \in (L^2(\Omega))^2$ and $f_\lambda \in L^2(\Omega)$, assume in addition*

$$\eta_0\mathcal{C}_K - \mathcal{C}_1\,|\boldsymbol{u}_h|_1 > 0 \tag{18}$$

$$\mathcal{M}_a - \mathcal{C}_2\mathcal{M}_b\,|\boldsymbol{u}_h|_{1,\infty} > 0 \tag{19}$$

the discrete TVP problem (17) has a unique solution $(\tilde{\boldsymbol{u}}_h,p_h) = (\lambda_h,\boldsymbol{u}_h,p_h) \in \mathbb{W}_h\times\mathbb{Q}_h$. Furthermore, the error estimate satisfies the best approximation, stated as

$$|\boldsymbol{u}-\boldsymbol{u}_h|_{1,\infty}^2 \leq (2+2\tilde{\mathcal{C}}_{\boldsymbol{u},\boldsymbol{u}})\inf_{\boldsymbol{v}_h\in\mathbb{V}_h}|\boldsymbol{u}-\boldsymbol{v}_h|_{1,\infty}^2 + \tilde{\mathcal{C}}_{\boldsymbol{u},\lambda}\inf_{\xi_h\in\mathbb{T}_h}\|\lambda-\xi_h\|_1^2 + \mathcal{C}_{\boldsymbol{u},p}\inf_{q_h\in\mathbb{Q}_h}\|p-p_h\|_0^2 \tag{20}$$

$$\|\lambda-\lambda_h\|_0^2 \leq \tilde{\mathcal{C}}_{\lambda,\boldsymbol{u}}\inf_{\boldsymbol{v}_h\in\mathbb{V}_h}|\boldsymbol{u}-\boldsymbol{v}_h|_{1,\infty}^2 + (2+2\tilde{\mathcal{C}}_{\lambda,\lambda})\inf_{\xi_h\in\mathbb{T}_h}\|\lambda-\xi_h\|_1^2 \tag{21}$$

where $\tilde{\mathcal{C}}_{\boldsymbol{u},\boldsymbol{u}},\tilde{\mathcal{C}}_{\boldsymbol{u},\lambda},\tilde{\mathcal{C}}_{\boldsymbol{u},p},\tilde{\mathcal{C}}_{\lambda,\boldsymbol{u}}$, and $\tilde{\mathcal{C}}_{\lambda,\lambda}$ are constants dependent on $\eta_0,\eta_\infty,\tau_\infty,\mathcal{M}_a,\mathcal{M}_b,k,\beta,\mathcal{C}_K,d$, $|\boldsymbol{u}|_1$, $|\boldsymbol{u}|_{1,\infty}$, $|\boldsymbol{u}|_{0,\infty}$, $|\boldsymbol{u}_h|_{1,\infty}$, $|\boldsymbol{v}_h|_{1,\infty}$, and $\|\xi_h\|_0$.

The choice of FE spaces for the approximation of TVP problem (6) is done w.r.t. the saddle point character related to incompressibility only, while microstructure is collocated with velocity. In order to deal with remaining challenges, i.e. the dependency of solution on k (regularization) and the lack of coercivity

of $a_\lambda(\cdot)(\cdot,\cdot)$ in a strong norm, we use higher order stabilized FEM. Indeed, we choose the pair Q_2/P_1^{disc} for velocity and pressure, and Q_2 for microstructure (see Figure 1) with inter-element gradient jumps as a stabilizing bilinear form supplementing the microstructure equation [1, 10] i.e.

$$j_\lambda(\lambda_h, \xi_h) \;= \sum_{E\in\mathcal{E}_i} \gamma_\lambda |E|^2 \int_E [\nabla\lambda_h]\,[\nabla\xi_h]\, d\sigma. \tag{22}$$

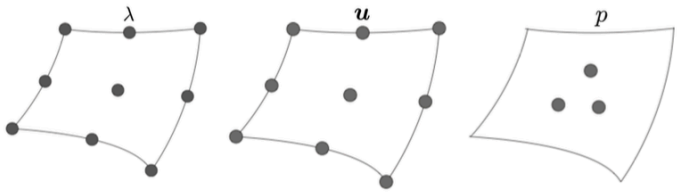

FIGURE 1. FEM choice for TVP problem: Higher order FEM discretization $Q_2/Q_2/P_1^{disc}$.

ADAPTIVE COMBINED DISCRETE NEWTON'S/MONOLITHIC GEOMETRIC MULTIGRID SOLVER

This section is concerned with an adaptive combined discrete Newton's and Monolithic Geometric Multigrid (MGMG) solver for the approximate nonlinear TVP problem (17). The solver has two folds w.r.t. adaptivity, the one related to discrete Newton's method via the step-size in divided difference for the Jacobian calculation, while the other is related to linear multigrid solver via the dependency of its accuracy/convergence on the accuracy/convergence of nonlinear solver.

Let $\{\varphi_i, i = 1, 2, \ldots, \mathtt{dim}\mathbb{W}_h\}$ and $\{\psi_i,\ i = 1, \ldots, \mathtt{dim}\mathbb{Q}_h\}$ be basis for $\mathbb{W}_h$ and $\mathbb{Q}_h$ spaces, respectively. Thus, the vector solution $\mathcal{U} = (\lambda_h, \boldsymbol{u}_h, p_h) = (\tilde{\boldsymbol{u}}_h, p_h) \in \mathbb{W}_h \times \mathbb{Q}_h$ is expressed as

$$\mathcal{U} = \sum_{i=1}^{\mathtt{dim}\mathbb{W}_h} \tilde{\boldsymbol{u}}_i\varphi_i + \sum_{i=1}^{\mathtt{dim}\mathbb{Q}_h} p_i\psi_i \tag{23}$$

and nonlinear discrete residuals for the system (17) are denoted by $\mathcal{R}(\mathcal{U}) \in \mathbb{R}^{\mathtt{dim}\mathbb{W}_h + \mathtt{dim}\mathbb{Q}_h}$

$$R(\mathcal{U}) = (\mathcal{R}_\lambda(\lambda_h, \boldsymbol{u}_h), \mathcal{R}_{\boldsymbol{u}}(\lambda_h, \boldsymbol{u}_h, p_h), \mathcal{R}_p(\boldsymbol{u}_h, p_h)) = (\mathcal{R}_{\tilde{\boldsymbol{u}}}(\tilde{\boldsymbol{u}}_h, p_h), \mathcal{R}_p(\tilde{\boldsymbol{u}}_h, p_h)) \tag{24}$$

We present concisely the main steps for the solver in Algorithm 1.

Algorithm 1: Discrete adaptive Newton using adaptive step-length

Result: $\mathcal{U}^{l+1} = \mathcal{U}^l - \omega_l \delta\mathcal{U}^l$, $\omega_l \in (0, 1]$
$r_0 = \left\|\mathcal{R}(\mathcal{U}^0)\right\|$, $\varepsilon_0^{\pm}$;
while $r_l \geq r_c$;
do

(i) **Calculate convergence rate** $r_l = \frac{\|\mathcal{R}(\mathcal{U}^l)\|}{\|\mathcal{R}(\mathcal{U}^{l-1})\|}$;

(ii) **Step-length size update** $\varepsilon_{l+1}^{\pm} = g(r_l)\varepsilon_l^{\pm}$;

(iii) **Calculate FD Jacobian** $\left[\mathcal{J}(\mathcal{U}^l)\right]_{ij} \approx \frac{\left(\mathcal{R}_i(\mathcal{U}^l + \varepsilon_l^+ \boldsymbol{e}_j) - \mathcal{R}_i(\mathcal{U}^l - \varepsilon_l^- \boldsymbol{e}_j)\right)}{\varepsilon_l^+ + \varepsilon_l^-}$;

(iv) **Solve via MGMG** $\mathcal{J}(\mathcal{U}^l)\delta\mathcal{U}^l = \mathcal{R}(\mathcal{U}^l)$;

end

Remark 3. *The damping parameter ω_l is set to unity, since it is not enough for convergence of the Algorithm 1. The feedback singularity is given by the rate of the actual residual convergence r_l in (i). Thus, the update function $g(r_l) = (0.7 + e^{1.5x})(4.14 + 0.2e^{1.5x})^{-1}$ in (ii) is chosen in a way to allow for bigger step-length parameter $\varepsilon^{\pm}$ to remove numerical instabilities and a smaller one in the region of quadratic convergence. Some numerical tests for unit square Bingham flow benchmark can be found in [11]. The finite difference scheme in (iii) is made to switch flexibly between backward finite difference ($\varepsilon_l^+ = 0$), forward finite difference ($\varepsilon_l^- = 0$), and central finite difference ($\varepsilon_l^- = \varepsilon_l^+ \neq 0$) based on the type of singularity of the Jacobian and the accuracy requirement for its calculation. To solve the linear system (iv), we use monolithic*

adaptive geometric multigrid methods, where the convergence of linear solver is made to match the optimal accuracy of the nonlinear solver by means of the rate of the actual residual convergence [1]. The analysis of the global convergence property of the algorithm and the smoothing property of multigrid goes beyond the interest of this paper and will be reported separately.

On one hand, geometric multigrid methods (GMG) damp both high- and low-frequency components of errors using effectively the complementary processes of coarse-grid correction and smoothing/relaxation. On other hand, Local Multilevel Pressure Schur Complement (LMPSC) scheme solve exactly the local saddle-point problem on subdomains and perform an overlapping block-Gauss–Seidel iteration. In the following, we give the principle of GMG via multi level algorithm and its corresponding components in the context of FEM discretization of approximate TVP problem (17).

Let $\{\mathcal{T}_{h_k}\}$ be a familly of hierarchy multilevel triangulations associated with mesh size h_k, i.e. each element on level triangulations $\mathcal{T}_{h_{k-1}}$ is split into $\sigma_i(K)_{i=1,\dots,2^d}$, $d=2$, new elements to get level triangulations $\mathcal{T}_{h_k}$ (Figure 2). We set $\mathcal{W}_k := \mathbb{R}^{\dim\mathbb{W}_{h_k}}$, $\mathcal{Q}_k := \mathbb{R}^{\dim\mathbb{Q}_{h_k}}$, $\mathcal{V}_k := \mathcal{W}_k \times \mathcal{Q}_k$ and let $\boldsymbol{\mathcal{I}}_k^{k-1}$ and $\boldsymbol{\mathcal{I}}_{k-1}^{k}$ denote the grid transfer operators, $\boldsymbol{\mathcal{I}}_k^{k-1} : \mathcal{V}_k \longrightarrow \mathcal{V}_{k-1}$ and $\boldsymbol{\mathcal{I}}_{k-1}^{k} : \mathcal{V}_{k-1} \longrightarrow \mathcal{V}_k$. The number of smoothing steps in Figure 2, i.e. pre- and post-smoothing, are denoted by $\nu_1 \geq 0$ and $\nu_2 \geq 0$, respectively.

Given initial guess $\delta\mathcal{U}_0$, the k^{th}-level iteration $MG(k, \delta\mathcal{U}_0, \mathcal{R})$ of MG algorithm is an approximation to $\delta\mathcal{U}_k$ which is solution of

$$\mathcal{J}_k \delta\mathcal{U} = \mathcal{R} \tag{25}$$

One step can be described concisely throughout multi-level algorithm in Figure 2.

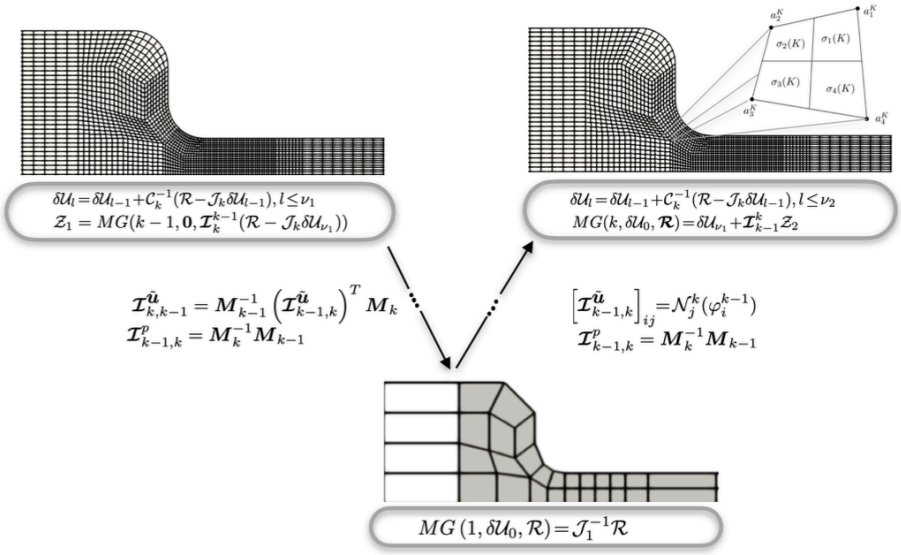

FIGURE 2. Monolithic Geometric MG solver: Multi-grid algorithm on a mesh-slice of 4:1 contraction configuration.

Smoothing steps in multigrid algorithm (Figure 2) are performed using LMPSC schemes in block Gauss-Seidel iteration manner, where the choice of blocks for the system (25) is based on incompressibility constraint/equivalently on the pressure degrees of freedom. Since the choice of blocks is based on incompressibility constraint and due to no-coupling between pressure and microstructure, we collocate the microstructure and velocity.

To set local sub-problems, we introduce prolongation matrices $\boldsymbol{\mathcal{P}}_K^{\tilde{\boldsymbol{u}}}$, $\boldsymbol{\mathcal{P}}_K^{p}$, and $\boldsymbol{\mathcal{P}}_K$ defined on spaces of variables values $\mathcal{W}_K := \mathbb{R}^{\dim\mathbb{W}_K}$, $\mathcal{Q}_K := \mathbb{R}^{\dim\mathbb{Q}_K}$, and $\mathcal{V}_K := \mathcal{W}_K \times \mathcal{Q}_K$, respectively. Then, the bolck Gauss-Seidel iteration reads

$$\mathcal{U}^{k+1} = \mathcal{U}^k - \omega_k \sum_{K \in \mathcal{T}_h} \boldsymbol{\mathcal{P}}_K \left(\boldsymbol{\mathcal{P}}_K^{\mathrm{T}} \left(\frac{\partial \mathcal{R}(\mathcal{U}^k)}{\partial \mathcal{U}}\right) \boldsymbol{\mathcal{P}}_K\right)^{-1} \boldsymbol{\mathcal{P}}_K^{\mathrm{T}} \mathcal{R}(\mathcal{U}^k). \tag{26}$$

Note that local sub-problems are of saddle point type. Furthermore, due to jump stabilization contributions, local matrices for microstructure and velocity are deduced form patch of elements, i.e. the designated element by pressure and all its nieghbors. One might only include the jump contributions within the designated element by pressure to have a standard size of local sub-problems [1, 12].

NUMERICAL SIMULATIONS OF THIXOTROPIC FLOW

In this section, we present numerically thixotropic flow behavior in two configurations: Firstly, in a simple enough geometry for laboratory experiments and numerical simulations, couette flow. Secondly, a close enough geometry to industrial applications, 4:1 contraction flow. For this purpose, we select Houška's material model from thixotropic collection given in Table I. For the former, we study the type of transitions between quasi-static and intermediate regimes w.r.t. intensity of breakdown parameter, while in the second we analyze the flow behavior in the vicinity of walls of the channel in downstream as well as across the contraction zone.

Thixo-viscoplastic Couette flow

We start by revisiting the numerical study of Couette flow using constitutive model for quasi-static and intermediate flows of powder material [13], with the aim to analyze the type of transitions between quasi-static and intermediate flow regimes by introducing thixotropy. We should make it clear that our revisit is purely theoretical in the absence of experiment data for thixotropic material.

The geometry constitute of two cylinders (concentric), the inner cylinder with radius, r_{in}, while the outer cylinder with radius, r_{out}, with radii ratio, ς, such that $r_{\text{in}} = \varsigma/(1-\varsigma)$ and $r_{\text{out}} = 1/(1-\varsigma)$. The material is sheared in the gap using the rotation speed of inner cylinder and no moving outer cylinder Figure 3 (RIGHT).

Figure 3 (LEFT) shows comparison of numerical solutions with experimental data. We calculate on the rotating cylinder, the ratio of average shear to normal stresses which we plot with respect to shear rate. In this first test, the experimental data itself was used as an input in the model in order to validate our new numerical tools.

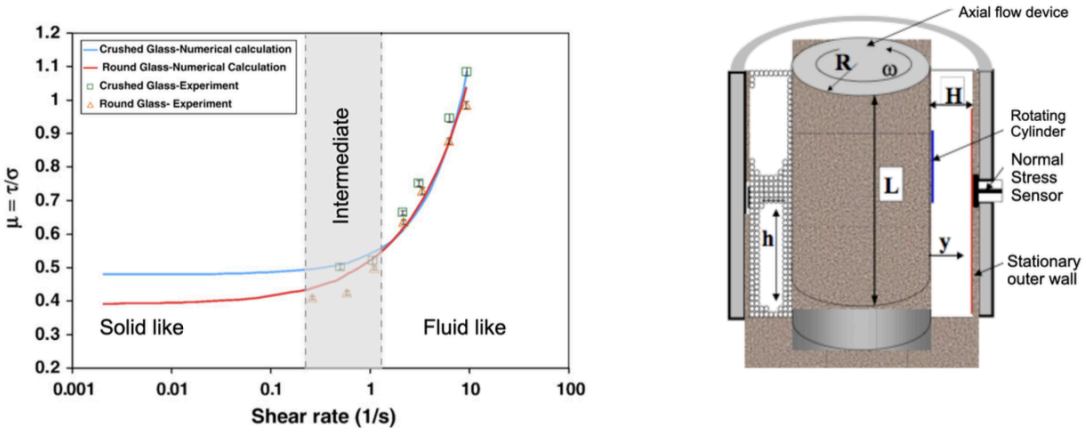

FIGURE 3. Couette flow: Comparison of numerical solution to experiments (LEFT) and Couette device (RIGHT) [13].

The new developed numerical methods do not introduce errors to experimental data Figure 3 (LEFT). Furthermore, Figure 3 (LEFT) exposes a shear-rate independent (solid-like), shear rate dependent (fluid-like), shear stress, and a transition region which is not yet well studied. In what follows, we activate thixotropy using Houška's thixotropic model as straightforward extension of the constitutive equation as a linear combination of shear-rate independent and shear-rate dependent stress with microstructure, providing extra parameters to investigate the type of transitions between solid-like and fluid-like regions.

Next numerical simulation, we present the cutlines of velocity and microstructure along radial directions w.r.t. breakdown parameter in Figure 4, similar as in [14].

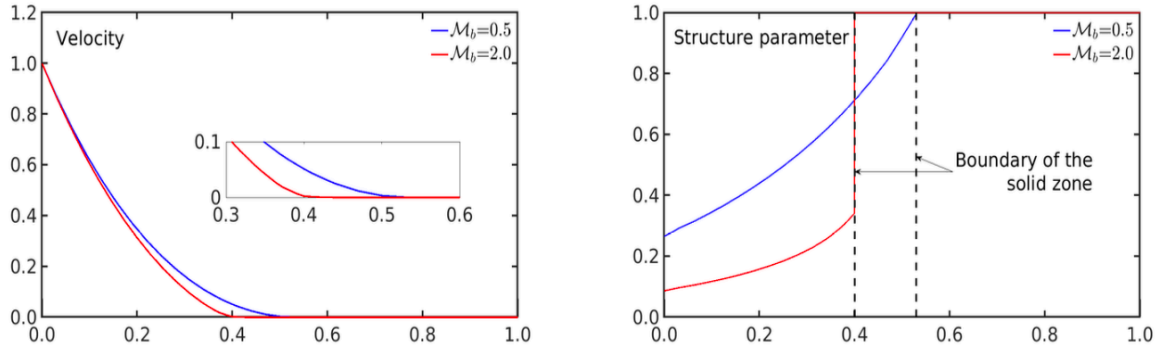

FIGURE 4. Thixo-viscoplastic Couette flows: Cutlines of velocity and microstructure along radial directions, $\theta = c$, $c \in [0, 2\pi]$, w.r.t. breakdown parameter, $\mathcal{M}_b$, for Houška's model, where remaining parameters are set to $\mathcal{M}_a = 1.0$, $\eta_0 = 1.0$, $\tau_0 = 2.0$, $\eta_\infty = 1.0$, $\tau_\infty = 1.0$, $n = 1$, and $k = 10^4$.

A smooth transition from fluid-like regimes to solid-like regimes is given with small values of breakdown parameter, while a sharp transition is induced for higher breakdown parameter. Microstructure profiles match with fluid-like and solid-like regions indicated by velocity profiles. Furthermore, the transition points for "localization" (lower breakdown parameter, $\mathcal{M}_b = 0.5$) and "shear banding" (higher breakdown parameter $\mathcal{M}_b = 2.0$) for velocity and microstructure match, which express once more the accuracy of the quasi-Newtonian modeling approach modulo sufficient higher regularization parameter.

Thixo-viscoplastic contraction flow

In this experiment, we use 4:1 contraction configuration to analyze TVP material. Our aim is to revisit flow characteristics taking in consideration material's thixotropy.

The breakdown parameter, $\mathcal{M}_b$, effect on flow characteristics is shown in Figure 5.

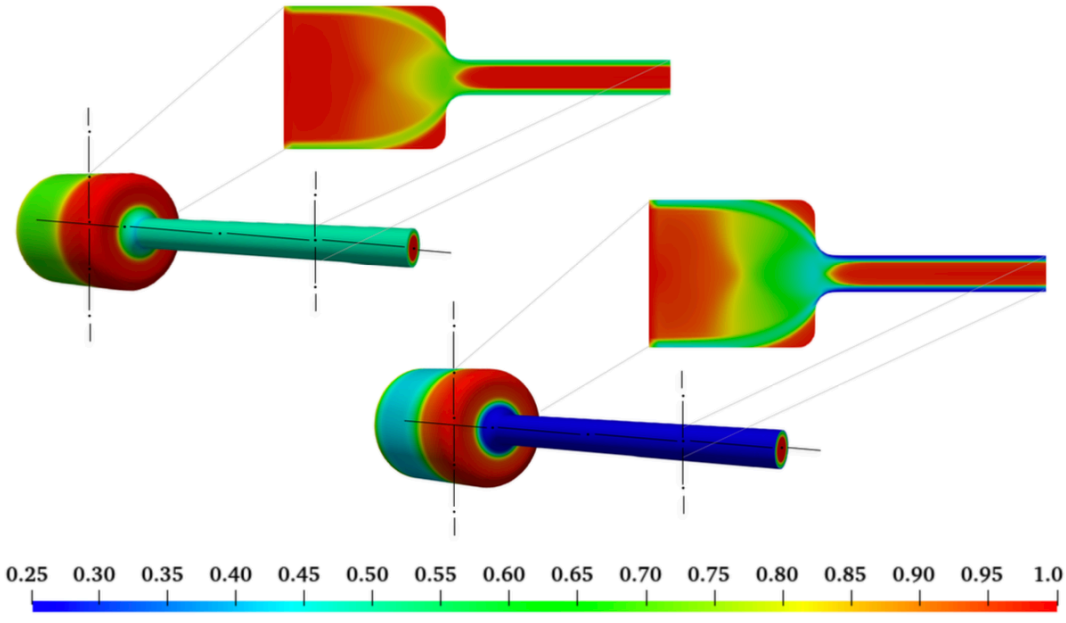

FIGURE 5. Thixo-viscoplastic flows in contractions: Microstructure λ distribution with respect to breakdown parameter, $\mathcal{M}_b = 1.0/\mathcal{M}_b = 2.0$ (TOP/BOTTOM). The remaining model parameters are set to $\mathcal{M}_a = 1.0$, $\tau_0 = 0.0$, $\eta_\infty = 1.0$, $\tau_\infty = 2.0$, $\eta_0 = 1.0$, and $k = 10^4$.

It is noticeable, in (Figure 5), that the induced thickness of rejuvenation layers is an outcome of breakdown parameter. This is why thixotropic material remains smoothly flowing and not resting along channel. As a consequence, further studies concerning the necessity of extra lubrication as well as the optimization of restart pressure settings are required.

Furthermore, three unyielded zones, near corners, entrance part of upstream channel, and center of downstream channel, are separated with one yielded zone. The yielded separation zone is categorized as a smooth for lower breakdown parameter and sharp for higher breakdown parameter. The observed non-emerging upstream's and downstream's unyielded zones is most probably due to lack of elasticity in the model. In fact, elasticity allows for a continuous flowing of the material across contraction section, which is not the case for TVP material. The answer relay on the investigation of thixo-elastoviscoplastic material via more general models.

SUMMARY

We presented FEM quasi-Newtonian modeling and simulation of TVP flows as straightforward way to generalize standard FEM settings of N-S equations. The microstructure is integrated within the nonlinear viscosity as a feedback response for the evolution competitive process of aging/buildup and rejuvenation/breakdown of thixotropic material. Firstly, we provided wellposedness results for TVP problem, then established the best approximation. The energy inequality presents some coarseness in terms of extra regularity requirement for velocity, nonoptimality of microstructure estimate, and dependency of its constants on regularization, which we dealt with stabilized higher order FEM approximations. In fact, we used higher order stable Stokes pair Q_2/P_1^{disc} FE approximations for velocity/pressure and higher order Q_2 FE approximation for microstructure field with a penalized inter-element gradient jump to enhance discrete weak energy norm to an equivalent one-norm. Secondly, the discrete nonlinear TVP system is solved using adaptive combined discrete Newton's monolithic geometric multigrid solver. The adaptivity within the discrete Newton's method is done through the step-size in divided difference for Jacobian calculation, while the accuracy of linear geometric multigrid solver is made in accordance to the accuracy requirement for nonlinear solver. The resulting solver is robust w.r.t. regularization parameter as a must for an accurate solution for quasi-Newtonian modeling of TVP problem. Lastly, we revisited Couette flow and 4:1 contraction flow by activating thixotropy. For the former, we correlated the constitutive models of shear rate independent and shear rate dependent stress using microstructure, enabling analysis of type of transitions between solid-like and fluid-like regimes. For 4:1 contraction flow, we showed that thixotropy induces extra breakdown layers in the vicinity of walls, consequently optimizing the restart pressure settings.

ACKNOWLEDGMENTS

- The authors acknowledge the funding provided by the "Deutsche Forschungsgemeinschaft (DFG, German Research Foundation) - 446888252".
- The authors acknowledge the financial grant provided by the "Bundesministerium für Wirtschaft und Klimaschutz aufgrund eines Beschlusses des Deutschen Bundestages" through " AiF-Forschungsvereinigung: Forschungs- Gesellschaft Verfahrens Technik e. V. - GVT" under the IGF project number "20871 N".
- We would also like to gratefully acknowledge the support by LSIII and LiDO3 team at ITMC, TU Dortmund University, Germany.

REFERENCES

1. A. Ouazzi, *Finite Element Simulation of Nonlinear Fluids: Application to Granular Material and Powder* (Shaker Verlag, 2006).
2. A. Ouazzi, N. Begum, and S. Turek, "Newton–multigrid FEM solver for the simulation of quasi–Newtonian modeling of thixotropic flows," in *Numerical Methods and Algorithms in Science and Engineering*, Vol. 700 (-, 2021).
3. T. Papanastasiuo, "Flow of materials with yield," J. Rheol. **31**, 385–404 (1987).
4. W. Worrall and S. Tuliani, "Viscosity changes during the aging of clay-water suspensions," Trans. Brit. Ceramic Soc. **63**, 164–185 (1964).
5. P. Coussot, Q. D. Nguyen, H. T. Huynh, and D. Bonn, "Viscosity bifurcation in thixotropic, yielding fluids," J. Rheol. **46**, 573–589 (2002).
6. M. Houška, *Engineering aspects of the rheology of thixotropic liquids*, PhD Thesis, Faculty of Mechanical Engineering, Czech Technical University of Prague (1981).
7. K. Dullaert and J. Mewis, "Transient phenomena in thixotropic systems," J. Non-Newton. Fluid Mech. **139**, 31–30 (2006).
8. N. Begum, A. Ouazzi, and S. Turek, "Fem simulations for thixo-viscoplastic flow problems; wellpoasedness results," Tech. Rep. (Fakultät für Mathematik, TU Dortmund, 2021) ergebnisberichte des Instituts für Angewandte Mathematik, Nummer 653, 2022.
9. N. Begum, A. Ouazzi, and S. Turek, "Fem simulations for thixo-viscoplastic flow problems; error analysis," Tech. Rep. 656 (Faculty of Mathematics, TU Dortmund University, 2022).
10. S. Turek and A. Ouazzi, "Unified edge–oriented stabilization of nonconforming FEM for incompressible flow problems: Numerical investigations," Journal of Numerical Mathematics **15**, 299–322 (2007).
11. A. Fatima, S. Turek, A. Ouazzi, and A. Afaq, "An adaptive discrete Newton method for regularization–free Bingham model," Tech. Rep. 635 (Faculty of Mathematics, TU Dortmund University, 2021).
12. A. Ouazzi and S. Turek, "Efficient multigrid and data structures for edge–oriented FEM stabilization," in *Numerical Mathematics and Advanced Applications Enumath 2005* (Springer, 2006) pp. 520–527, iSBN-10 3-540-34287-7.
13. M. Kheiripour Langroudi, S. Turek, A. Ouazzi, and G. Tardos, "An investigation of frictional and collisional powder flows using a unified constitutive equation," Powder Technology **197**, 91–101 (2009).
14. M. Jenny, S. Kiesgen de Richter, N. Louvet, S. Skali-Lami, and Y. Dossmann, "Taylor-couette instability in thixotropic yield stress fluids," Phys. Rev. Fluids **2**, 023302 (2017).
15. P. Moller, A. Fall, V. Chikkadi, D. Derks, and D. Bonn, "An attempt to categorize yield stress fluid behaviour," Phil Trans. R. Soc. A **367**, 5139–5155 (2009).
16. A. Mujumdar, A. N. Beris, and A. B. Metzner, "Transient phenomena in thixotropic systems," J. Nonnewton. Fluid Mech. **102**, 157–178 (2002).